Nuclear demagnetization for ultra-low temperatures

Nuclear demagnetization for ultra-low temperatures

Satoshi Abe[a,*], Koichi Matsumoto[a]

[a]*Department of Physics, Kanazawa University, Kanazawa 920-1192, Japan*

Abstract

Nuclear demagnetization is one of the most successful methods of cooling an appreciable amount of matter to the lowest temperatures. The principle of nuclear demagnetization is the same as that of the adiabatic demagnetization of a paramagnetic salt; however, there is a significant difference in practice. This article focuses on nuclear demagnetization refrigeration used in experiments at millikelvin and much lower temperatures. After a brief overview of the basic principle and methods, typical requirements of the refrigerants are described from the view point of experiments. The heat switch and thermometry used in nuclear demagnetization experiments are also discussed.

Keywords: Nuclear Demagnetization, Ultra-low temperature

Adiabatic demagnetization utilizing nuclear instead of electronic magnetic moments is used to extend the temperature range available for physical measurements into the sub-millikelvin region. Nuclear demagnetization cooling was proposed by Goter[1] in 1934, but many technical problems prevented its application until 1956 when Kurti et al. reduced the nuclear temperature to about 1 μK for a few minutes[2]. The development of the ^{3}He–^{4}He dilution refrigerator and the superconducting magnet were successful applications of nuclear demagnetization. The lowest temperatures of atoms, the nanokelvin or picokelvin range, can be achieved by the techniques of laser cooling and magneto-optical trapping employed in the investigation of the Bose–Einstein condensation of atoms. However, nuclear demagnetization has remained the dominant technique for cooling the nuclear spins and conduction electrons of solids and liquids down to sub-millikelvin temperatures. Dry nuclear demagnetization refrigerator without liquid helium has been developed because a ^{3}He–^{4}He dilution refrigerator has become practical using a mechanical cryocooler. In this article, we focused on our nuclear demagnetization refrigerator with liquid helium and the techniques used therein.

1. Principle of nuclear demagnetization

The basic principle of nuclear demagnetization cooling is the same as that of adiabatic demagnetization of a paramagnetic salt[3]. For a perfect nuclear paramagnet in which interactions between nuclear moments are ignored, the entropy S and the magnetic heat capacity $C_{\rm B}$ of N moments at temperature T in magnetic field B are given by

$$\frac{S}{Nk_{\rm B}} = \frac{x}{2I}\coth\frac{x}{2I} - \frac{2I+1}{2I}x\coth\frac{2I+1}{2I}x + \log\left(\sinh\frac{2I+1}{2I}x/\sinh\frac{x}{2I}\right) \quad (1)$$

$$\frac{C_{\rm B}}{Nk_{\rm B}} = \left(\frac{\frac{x}{2I}}{\sinh\frac{x}{2I}}\right)^2 - \left(\frac{\frac{2I+1}{2I}x}{\sinh\frac{2I+1}{2I}x}\right)^2, \quad (2)$$

$$x \equiv \frac{\mu_{\rm n}g_{\rm n}IB}{k_{\rm B}T},$$

where $\mu_{\rm n}$, $g_{\rm n}$, and I are the nuclear magneton, the nuclear g-factor, and the nuclear angular momentum, respectively. Since the nuclear magnetic moment is about 2000 times smaller than the electronic magnetic moments, the Zeeman energy $\mu_{\rm n}g_{\rm n}IB$ is usually smaller than $k_{\rm B}T$ even though there is a large value of $B/T \sim 1000$ T/K, which can be achieved using a dilution refrigerator and superconducting magnet. Therefore, the entropy S and heat capacity $C_{\rm B}$ of n moles of nuclear moments are given by

$$S = nR\log(2I+1) - \frac{n\lambda}{2\mu_0}\frac{B^2}{T^2}, \quad (3)$$

$$C_{\rm B} = \frac{n\lambda B^2}{\mu_0 T^2}, \quad (4)$$

where R is the gas constant, μ_0 is the permeability, and $\lambda = N_{\rm A}\mu_0\mu_{\rm n}^2 g_{\rm n}^2 I(I+1)/3k_{\rm B}$ is the molar Curie constant. The contribution to the entropy and the heat capacity from the conduction electrons and the lattice can be ignored at temperatures of the nuclear demagnetization.

If the interactions between the nuclear moments cannot be ignored, B in equations above should be replaced with an effective magnetic field $B_{\rm eff}$:

$$B_{\rm eff} = \sqrt{B^2 + b^2}. \quad (5)$$

*Corresponding author. E-mail address: abesi@staff.kanazawa-u.ac.jp

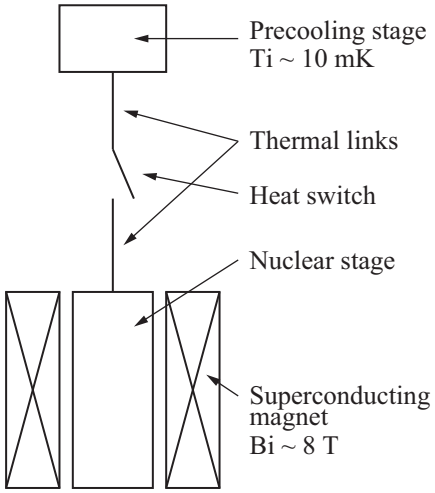

Figure 1: Schematic diagram of a nuclear demagnetization cryostat.

The effective internal field b of the nuclear moments is about $(2000)^2$ times smaller than that of the electronic moments. Thus, the lowest temperature of nuclear demagnetization can reach the microkelvin or nanokelvin range.

2. Methods of nuclear adiabatic demagnetization

A schematic diagram of a cryostat for nuclear demagnetization is illustrated in Fig. 1. The nuclear demagnetization is usually performed with a single-shot device. After the demagnetization is carried out to the lowest field, the refrigerant and attached sample are then warmed through heat leaks. In the 1960s, electronic adiabatic demagnetization was employed in the precooling stage for nuclear demagnetization. The ^{3}He–^{4}He dilution refrigerator, which has continuous cooling power down to about 10 mK, is used nowadays. A heat switch is needed between the precooling and nuclear stages for adiabatic demagnetization. The superconducting heat switch described in section 3.4 is usually used because of its high switching ratio of the thermal conductivity.

2.1. Heat of magnetization

The nuclear stage is magnetized from zero to $B_\mathrm{i} \sim 10$ T by a superconducting magnet while the heat switch is closed. From Eqs. 3 and 4, we find

$$TdS = C_\mathrm{B}dT - \frac{n\lambda}{\mu_0}\frac{B}{T}dB. \tag{6}$$

Thus, the heat of magnetization while the nuclear stage is cooled from a high temperature to $T_\mathrm{i} \sim 10$ mK in a constant magnetic field $B = B_\mathrm{i}$ is

$$\Delta Q(B = B_\mathrm{i}) = -\int TdS = -\int_\infty^{T_\mathrm{i}} C_\mathrm{B}dT = \frac{n\lambda B_\mathrm{i}^2}{\mu_0 T_\mathrm{i}}. \tag{7}$$

In the case of isothermal magnetization at $T = T_\mathrm{i}$, we obtain the heat of magnetization as

$$\Delta Q(T = T_\mathrm{i}) = -\int TdS = \int_0^{B_\mathrm{i}} \frac{n\lambda}{\mu_0}\frac{B}{T_\mathrm{i}}dB = \frac{n\lambda B_\mathrm{i}^2}{2\mu_0 T_\mathrm{i}}. \tag{8}$$

Thus, half of the heat should be absorbed by the precooling stage in isothermal magnetization. However, it is not practical to magnetize isothermally in the nuclear demagnetization experiment using a superconducting magnet. The cooling power of the dilution refrigerator used for the precooling stage is proportional to T^2. Thus, it is better to increase the magnetic field quickly from zero to B_i, although the temperature of the nuclear stage becomes high. This can reduce the consumption of liquid helium in the main bath due to ohmic losses in the current leads to the magnet when the superconducting magnet is not in persistent mode.

The precooling time depends on the amount and material of the nuclear refrigerant, and the cooling power of the precooling stage. We find the heat of magnetization is 32 mJ/mole for copper nuclei by inserting numerical values of $B_\mathrm{i} = 10$ T, $T_\mathrm{i} = 10$ mK, and $\lambda = 4.0 \times 10^{-12}$ Km^3/mole into Eq. 7. The cooling power of the ^{3}He–^{4}He dilution refrigerator is approximately tens of microwatts at 10 mK. Thus, it takes several days to precool 100 mol of copper nuclear stage in a magnetic field of 10 T down to an initial temperature about 10 mK.

2.2. Temperature difference between nuclear spins and conduction electrons

At low temperatures achieved by nuclear demagnetization, it is meaningful to separate the two temperatures of the nuclear spins T_n and the conduction electrons T_e, because the spin-spin relaxation time τ_2 at which the nuclei reach thermal equilibrium among themselves is usually shorter than the spin-lattice relaxation time τ_1 at which equilibrium is established between nuclear spins and conduction electrons. The spin-lattice relaxation time τ_1 is defined by

$$\frac{d}{dt}\left(\frac{1}{T_\mathrm{n}}\right) = -\frac{1}{\tau_1}\left(\frac{1}{T_\mathrm{n}} - \frac{1}{T_\mathrm{e}}\right). \tag{9}$$

For most metals in a normal state, τ_1 is of the order of seconds at 10 mK, whereas τ_1 is days or weeks for insulators. Therefore, the metal should be used for nuclear demagnetization to cool conduction electrons and the lattice. The energy transfer proceeds through the hyperfine interaction between the magnetic moments of nuclei and conduction electrons. Only the electrons near the Fermi energy level contribute to this, and the number of these electrons is proportional to T_e. Thus, a Korringa relation is found:

$$\tau_1\, T_\mathrm{e} = \kappa. \tag{10}$$

The Korringa constant κ is independent of temperature. It has a field dependence near $B \sim b$, but is approximately constant in $B \gg b$.

Nuclear refrigerant is selected considering the Korringa constant. The spin-lattice relaxation time τ_1 causes the temperature difference between T_n and T_e. From Eqs. 9 and 10, we find

$$\frac{dT_\mathrm{n}}{dt} = \dot{T}_\mathrm{n} = \frac{T_\mathrm{n}}{\kappa}\left(T_\mathrm{e} - T_\mathrm{n}\right). \tag{11}$$

During the nuclear demagnetization, the conduction electrons are cooled by the nuclear spins, and if the external heat leak is

absent, we obtain

$$\frac{d}{dt}\left(C_{\rm e}T_{\rm e} + C_{\rm B}T_{\rm n}\right) = 0, \tag{12}$$

where $C_{\rm e}$ is the heat capacity of the conduction electrons. Thus, we find

$$\Delta\dot{T} = \dot{T}_{\rm n} - \dot{T}_{\rm e} = \frac{T_{\rm n}}{\kappa'}\left(T_{\rm e} - T_{\rm n}\right), \tag{13}$$

where $\kappa' = \kappa C_{\rm e}/(C_{\rm B} + C_{\rm e})$. Usually, $C_{\rm e} \ll C_{\rm B}$, and then, $T_{\rm e}$ closely follows $T_{\rm n}$.

2.3. Effect of heat leak

In practice, we cannot avoid an external heat leak $\dot{Q}$. This heat leak causes a large temperature difference between $T_{\rm n}$ and $T_{\rm e}$ because it is first absorbed by the conduction electrons and lattice. From Eq. 11 and the rate $\dot{Q} = C_{\rm B}T_{\rm n}$ at which the nuclear spins can absorb heat from the conduction electrons, we obtain

$$\frac{T_{\rm e}}{T_{\rm n}} = 1 + \frac{\mu_0\kappa\dot{Q}}{n\lambda\left(B^2 + b^2\right)}. \tag{14}$$

Thus, to obtain the lowest temperature of conduction electrons, the demagnetization should be stopped at a field of

$$B_f(opt) = \sqrt{\frac{\mu_0\kappa\dot{Q}}{n\lambda}}, \tag{15}$$

assuming that $B_f(opt) \gg b$. In this final field, we obtain the relation

$$T_{\rm e}(B_f) = 2T_{\rm n}(B_f). \tag{16}$$

The actual final temperature of $T_{\rm e}(B_f)$ is higher than that given by Eq. 16 because the demagnetization process with an external heat leak is no longer adiabatic nor reversible. Rapid demagnetization can reduce the influence due to extra heat leaks but cause serious eddy current heating. The time Δt during which the nuclear spins warm from $T_{\rm n}(B_f)$ to some higher temperature $T_{\rm n}$ is given by

$$\Delta t = \frac{n\lambda\left(B_f^2 + b^2\right)}{\mu_0\dot{Q}}\left(\frac{1}{T_{\rm n}(B_f)} - \frac{1}{T_{\rm n}}\right), \tag{17}$$

where Eq. 4 has been employed. Thus, $\dot{Q}$ can be obtained from the time dependence of $1/T_{\rm n}$ after demagnetization, if $\dot{Q}$ is constant. To maintain the low temperature of $T_{\rm e}$ for measurements, the final demagnetization should stop at some higher field and the external heat leak $\dot{Q}$ should be as small as possible.

2.4. Origin of the external heat leak

The possible sources of the external heat leaks to the demagnetization stage are listed as follows.

1. mechanical vibration of the cryostat.
2. radio-frequency field and radiation penetrating the shields.
3. thermal conduction of supports and wirings.
4. eddy current heating by demagnetization.
5. internal heat generation.

The first three are common problems in low-temperature experiments and methods of counteracting these leaks have been developed by many researchers[3, 4, 5, 6]. For the same amount of external heat ΔQ, the entropy loss ΔS seriously increases with decreasing temperature because of the thermodynamic relation $\Delta Q = T\Delta S$. Thus, careful preparations are needed in nuclear demagnetization experiments.

The forth source results from the fact that the material of the nuclear refrigerant is a metal. From Faraday's law, the power dissipation due to eddy current for a metal cylinder when applying a magnetic field B parallel to the cylindrical axis is given as

$$\dot{Q}_{eddy} = \frac{\sigma AV}{8\pi}\left(\frac{\partial B}{\partial t}\right)^2, \tag{18}$$

where σ is the electrical conductivity, A is the cross-sectional area perpendicular to B, and V is the volume. Therefore, the eddy current heating of the metal is proportional to the cross-sectional area for a given rate of demagnetization. The area A is the area of the continuous part of the metal. Thus, if the metal is assembled from small cross-sectional parts that are insulated from each other, there is less eddy current heating than for a solid metal part having the same A and V. It is not desirable to reduce the electrical conductivity σ in order to reduce eddy current heating. At low temperature, the thermal conductivity k relates to the electrical conductivity σ according to the Wiedemann–Franz law:

$$k = \sigma\mathcal{L}\,T, \tag{19}$$

where $\mathcal{L} = 25 \times 10^{-9}$ WΩ/K^2 is the Lorentz constant. Thus, it would also reduce thermal conductivity needed to cool the investigated sample or cell.

The fifth source is thought to be the origin of the long-term heat leak. Amorphous solids such as glassy epoxies and glues are often used to provide thermal isolation, thermal contact, and mechanical support in the nuclear refrigerator. However, they are known to have very long time constants of structural relaxations, and may cause extra heat leaking over a long period. The time dependence of this heat leak is logarithmic, and it may thus take many weeks for the leak to become negligible[7]. Owing the differences in thermal contraction, stress acting at welds and solder joints also causes the heat leaks. An ortho-to-para transition of hydrogen containing in organic materials and metals also causes long-term extra heat leaks[8]. The exact source of the dominant long-term-relaxation heat leak is not well understood.

3. Cryostat for nuclear adiabatic demagnetization

3.1. Material for a nuclear refrigerant

The possible materials for nuclear refrigerant should have the following properties.

1. Large Curie constant λ allowing a large entropy reduction and a large heat capacity.
2. Small Korringa constant κ allowing the rapid formation of equilibrium between nuclear spins and conduction electrons.

3. High thermal conductivity, for the requirement of the thermal equilibrium in the nuclear stage over macroscopic distances.
4. No superconductivity in the final field, because electrons cannot contribute to the thermal conduction in the superconducting state.

Table 1 lists properties of some elements that can be used for nuclear demagnetization. The most common material used for the nuclear refrigerant is copper. Compound and alloys are not used except for hyperfine-enhanced nuclear paramagnets because of their poor thermal conductivities. In nuclear demagnetization experiments, the nuclear spins are usually used to refrigerate another system (for example, the electron, lattice, and another attached sample), which is a common application called the nuclear refrigerator. However, there is another type of nuclear demagnetization experiment called the nuclear cooling in which only the nuclear spin system of interest is cooled by demagnetization. By rapid demagnetization with duration much shorter than the spin–lattice relaxation time τ_1, the nuclear spin temperature T_n can be lowered significantly and then increased, while the conduction electron temperature stays at the initial temperature. The spontaneous ordering of nuclear spins has been studied for materials such as copper [9, 10], silver [11], rhodium [12], scandium [13], thallium [14], lithium [15], and hcp solid helium-3 [16], employing this nuclear cooling method and a double nuclear demagnetization cryostat. The second nuclear stage of the investigating nuclear material is cooled to its initial condition of $T_i \sim 100\,\mu$K and $B_i \sim 8$ T by the demagnetization of the first nuclear stage, and then, the nuclear spins can be cooled below the nuclear ordering temperature by demagnetization of the second stage.

3.2. Copper nuclear stage

Natural copper consists of approximately 69.1% of ^{63}Cu and 30.9% of ^{65}Cu, and both isotopes have nuclear spin $I = 3/2$. The effective nuclear Curie constant λ/v is 0.56 μK, where v =7.11 cm^3/mole is the molar volume. Figure 2 shows the nuclear entropy and heat capacity of copper as functions of temperature in various external magnetic fields. The first-order antiferromagnetic transition was observed at 50 nK[10]. Copper is the best material with which to reach microkelvin temperatures through nuclear refrigeration. Its important advantages are its high thermal conductivity and ready availability in various forms such as wires, rods, and plates.

When nuclear demagnetization was first applied using copper, it was believed that fine geometry of the refrigerant was essential to reduce eddy current heating by demagnetization. The first cryostat in which copper nuclear demagnetization and the ^{3}He–^{4}He dilution refrigerator were combined was constructed by Bergland et al.[17] in 1972. Their nuclear stage was made of 70,000 insulated 99.999%-pure copper wires with a diameter of 0.05 mm. The wires were folded with Araldite to eliminate vibrational heating due to the movement of loose wires. The copper nuclear stage is therefore sometimes called as a bundle even now. However, some excess materials such as the insulator of wires and epoxy used in folding the wires may cause

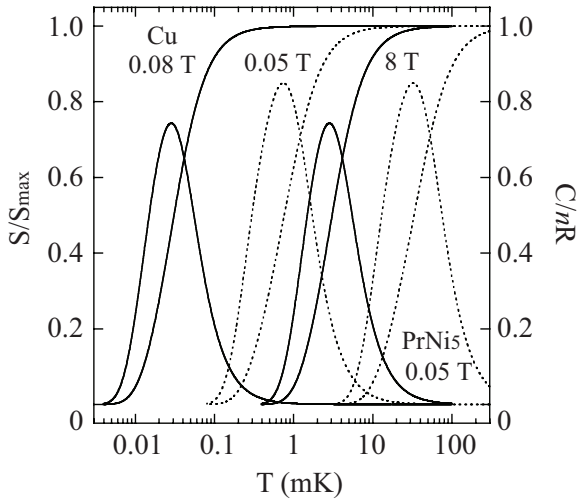

Figure 2: Nuclear entropy and heat capacity of copper (solid lines) and $PrNi_5$ (broken lines) as functions of temperature in various magnetic fields calculated using Eqs. 2 and 3. $S_{max} = n\mathrm{R}\log 4$ for copper and $S_{max} = n\mathrm{R}\log 6$ for $PrNi_5$, where R = 8.314 JK^{-1}mol^{-1} is the gas constant.

the residual heat leaks described in section 2.4. These materials also prevent the effective annealing of copper to improve the thermal conductivity of the nuclear stage, so that the typical residual resistivity ratio (RRR) of the nuclear stage of fine wires is usually a few hundred.

As described in section 2.2, the effective thermal relaxation time between nuclear spins and conduction electrons is of the order of hours below 1 mK. In addition, it sometimes takes much longer to cool the investigated sample because of the heat capacity of the sample and thermal resistance between the sample and nuclear stage. Thus, in practical experiments below 1 mK, the duration of demagnetization exceeds 10 h. For such a slow rate of demagnetization and ultra-low temperature, the nuclear stage needs to have sufficient thermal conductivity to achieve thermal equilibrium rather than fine geometry to reduce the eddy current heating. Recently, nuclear stage is usually made of copper rods or plates with diameter or thickness of a few millimeters. The rods or plates are spaced in an array so as not to be in contact with each other, and the ends of the rods or plates are welded to a copper experimental flange. There being no excess insulator or epoxy allows effective improvement of the thermal conductivity by annealing at higher temperature. One example of this nuclear stage was constructed by the Jülich group[18]. Their nuclear stage was made of 96 rectangular copper rods with a cross-section of 2×3 mm^2 and length of 245 mm, and RRR of 800 was obtained by annealing at 960 °C. The quantity of copper in the field is equivalent to 10 mol in a field of 8 T. They used this as the second nuclear stage of their double nuclear demagnetization cryostat, and obtained the lowest conduction electron temperature of 48 μK by demagnetizing from 8 T at 5 mK. Another example of a nuclear stage made of plates was provided by the Florida group[19]. Their demagnetization stage consisted of 3.2-mm-thick plates of 99.99% oxygen-free high-conductivity (OFHC) copper, containing 350 mol in total and 173 mol in a field of 8 T. A total of 19 plates with width

Table 1: Physical properties of possible candidates for nuclear demagnetization.

Refrigerant	Curie constant λ (10^{-12}Km^3/mole)	Korringa constant κ (sK)	spin-spin relaxation time τ_2 (μs)	effective internal field b (mT)	nuclear angular momentum I	super-conducting critical field H_c (mT)	References
Cu	4.05	1.1	80	0.36	3/2		[3, 9, 10]
Ag	0.0205	10		0.035	1/2		[3, 11]
Rh	0.013	8.0		0.044	1/2	0.0034	[3, 12]
Sc	13.5	0.09		0.22	7/2		[13]
Tl	3.6	0.0044	30		1/2	20	[14]
Li	7.67	44		0.24	3/2		[15]
^{3}He	10.8				1/2		
In	17.4	0.086		250	9/2	30	[3]
Pt	0.17	0.030	1000		1/2		[3]
Nb	21.7	0.19			9/2	300	[3]
Al	8.68	1.8	30		5/2	10	[3]
V	15.9	1.8	30		5/2	10	[3]

ranging from 11 to 63 mm was bundled to the approximate form of a cylinder having length of 910 mm and diameter of 63 mm. Each plate was electro-beam welded to top and bottom flanges.

One massive piece of high-purity copper is sometimes used to make the nuclear stage including experimental flanges to obtain high thermal conductivity throughout the nuclear stage. Several tens of slits with width of more than 1 mm are cut along the longitudinal axis with a circular saw to reduce eddy current heating. The Bayreuth group made their nuclear stage by an electric discharge machining method for cutting 36 slits of 0.4 mm width in their nuclear stage of 78 mm diameter and 525 mm length, which is 278 mol in total and 104 mol in a field of 8 T[20]. Figure 3 shows a typical copper nuclear stage that has 230 mol in total and 93 mol in a field of 8 T in our laboratory. This nuclear stage with a top flange having a diameter of 96 mm and various holes for mounting experiments and thermometers was machined from one piece of OFHC copper. The main part of the stage is machined as an octagonal cross section with a diameter of nearly 80 mm, so that 56 slits of 1 mm width and 350 mm length can be easily cut in each interval of 2.5 mm with a circular saw. After machining, the nuclear stage is annealed for 72 h at 900 °C in a O_2 atmosphere of 10^2 Pa to increase RRR to above 1000. The top flange is gold plated to ensure thermal contact. The magnetic field in the region without slits and around the top flange ($z > 25$ cm in Fig. 3) is reduced to less than 5 mT by the field compensation of the superconducting magnet, so that the eddy current heating and the influence on experiments and thermometry are small. The eddy current heating by demagnetization is estimated to be $\dot{Q}_{eddy}/(\partial B/\partial t)^2 \sim 16$ [Ws^2/T^2]. After 1 week of precooling with the ^{3}He–^{4}He dilution refrigerator, the demagnetization is started from the initial conditions of $B_i = 8$ T and $T_i = 9$ mK. The rate of demagnetization is typically 1.4×10^{-4} T/s at the beginning, and reduced step by step to 1.0×10^{-6} T/s at the lowest temperature of ~200 μK.

3.3. Hyperfine enhanced nuclear refrigeration

The method of hyperfine enhanced nuclear refrigeration was theoretically proposed by Altshuler[21] in 1966, and put into practice by Andres and Bucher[22] in 1968. By the interaction of nuclear magnetic moments with electrons, which is called hyperfine interaction, the electrons produce a hyperfine field at the nucleus. Normally this field is small, but in singlet-ground-state ions, with high Van Vleck susceptibilities, a strong hyperfine field is caused by the external field. In zero magnetic field, the ions are in nonmagnetic singlet ground states, but in an applied field, the wave function of the ground state changes and induces a magnetic moment. This moment consequently produces a strong hyperfine field at the nucleus with an enhancement factor $\alpha = 1 + K$, where K is the Knight shift and α is usually $10 \sim 100$. We can use Eq. 2, replacing B with αB. Thus, a large entropy reduction and large nuclear heat capacity are expected for the hyperfine enhanced nuclear demagnetization. For a large value of α, it is necessary to have small energy separation between the singlet ground state and the first excited state, which gives a high Van Vleck susceptibility and a large hyperfine coupling constant. The best candidates are rare earth ions Pr^{3+} and Tm^{3+} because they have the lowest spin angular momentum $S = 1$, which reduces exchange interaction and allows lower temperatures before the spontaneous ordering of electronic moments. The lowest temperature is limited by the spontaneous ordering of nuclear spins, which usually occurs around 1 mK in hyperfine enhanced nuclear magnets. Thus, the lowest attainable temperature of the hyperfine enhanced nuclear demagnetization is about two orders of magnitude higher than that of copper.

One of the best hyperfine enhanced nuclear refrigerants is praseodymium nickel five ($PrNi_5$), which has nuclear angular momentum $I = 5/2$, an enhancement factor $\alpha = 12.2$, an internal field $b = 66$ mT, and a nuclear ordering temperature $T_c = 0.40$ mK. As shown in Fig. 2, the enhanced field αB at the nucleus allows a higher initial temperature T_i and a weaker

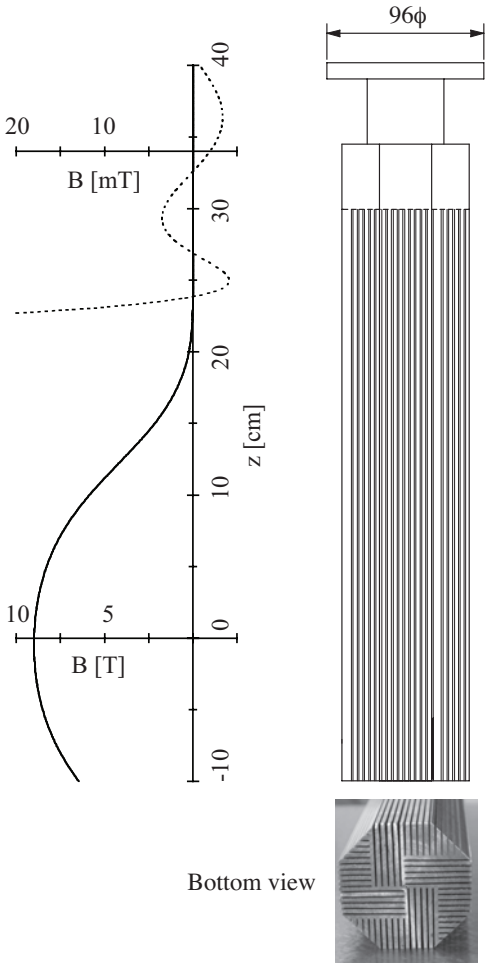

Figure 3: Schematic drawing of the copper nuclear stage and field profile of the superconducting magnet in our laboratory. The gold-plated top flange with diameter of 96 mm has various holes for mounting experiments and thermometers. The main part of the stage is machined as an octagonal cross section with a diameter of nearly 80 mm, so that slits can be easily cut with a circular saw. The magnetic field is reduced to less than 5 mT in the region $z > 25$ cm when $B =$ 9T at $z = 0$ cm. The field profile is plotted with two different field scales; the solid line relates to the lower scale and the dashed line to the upper magnified scale.

initial field B_i than in copper, so that a smaller amount of refrigerant is needed and a compact nuclear demagnetization cryostat can be constructed. The large cooling power of $PrNi_5$ is also used for the first nuclear stage of a double-stage nuclear demagnetization refrigerator[18]. The demagnetization of a few moles of $PrNi_5$ can precool the approximately 10 mol of the second copper stage to 5 mK in 8 T. As described in section 3.1, good thermal conductivity of the nuclear refrigerant is important. However, the thermal conductivity of $PrNi_5$ is limited by a lattice imperfection and even a good sample only has RRR of about $10 \sim 20$. The low-temperature thermal conductivity of $PrNi_5$ is almost the same as that of brass or CuNi[23]. Thus, it should not be used as a single solid piece of refrigerant but rather be thermally anchored to a good thermal conductor. This situation is similar to the demagnetization of a paramagnetic salt. $PrNi_5$ is usually formed into rods of diameter and length on the order of 6 and 100 mm respectively, and then thermally anchored along its entire length to copper wires having high thermal conductivity. The ends of the copper wires are welded to the experimental flange and the wires thus work as a thermal path of the nuclear refrigerant of $PrNi_5$. The $PrNi_5$ and copper wires are usually soldered with cadmium, which has a weaker critical field $B_c = 3$ mT of superconductivity. The demagnetization should be stopped before the critical field of solders is reached because of the poor thermal conductivity of the superconducting state.

3.4. Heat switch

In a low-temperature cryostat, it is often necessary to open and close thermal contact between different parts of the apparatus as desired. Many types of heat switches have been designed for this purpose, depending on the temperature regions[3, 4, 6]. For the temperature range below about 0.5 K, the most common type is a superconducting heat switch that uses the large difference in the thermal conductivity of the normal and superconducting states of metals. It can be operated ON/OFF by applying an external magnetic field stronger than the critical field of superconductivity. In the nuclear demagnetization cryostat, a heat switch is needed between the precooling state, usually in the mixing chamber of the ^{3}He–^{4}He dilution refrigerator, and the nuclear demagnetization stage as shown in Fig. 1. In the case of the double nuclear stage, another heat switch is often placed between the first and second nuclear stages.

The thermal conductivity of metal in the normal state k_n is proportional to temperature as described by Eq. 19, and the low-temperature electrical conductivity σ can be expressed by the resistivity at room temperature ρ_{RT} and the residual resistivity ratio R_{RRR} as $\sigma = R_{\mathrm{RRR}}/\rho_{\mathrm{RT}}$. Thus, k_{n} can be expressed as $k_{\mathrm{n}} = \mathcal{L} R_{\mathrm{RRR}}\, T/\rho_{\mathrm{RT}}$. In the superconducting state, at temperatures well below the transition temperature T_c, only phonons contribute significantly, and thermal conductivity is expressed as $k_{\mathrm{s}} = \frac{1}{3} C v \ell$. The heat capacity of phonons C is proportional to $(T/\Theta)^3$, where Θ is the Debye temperature. The phonon velocity v is of the order of 1000 m/s. The mean free path ℓ is determined by the average grain size, which is almost the same as the thickness or diameter of superconducting materials. Therefore,

Table 2: Physical properties of possible superconducting materials for the superconducting heat switch. T_c, H_c, Θ, and T_{melt} are the superconducting transition temperature, critical field, Debye temperature, and melting temperature, respectively.

material	T_c (K)	H_c (mT)	Θ (K)	T_{melt} (K)
Pb	7.19	80.3	105	601
Sn	3.72	30.9	200	505
In	3.40	29.3	108	430
Al	1.14	10.5	428	934
Zn	0.875	5.3	327	693

the switching ratio of the superconducting heat switch k_n/k_s is proportional to $1/T^2$. To obtain a large switching ratio, the superconducting material used for a heat switch should have three properties: low electrical resistivity at low temperatures to provide large RRR, high purity of the sample to increase k_n, and a large Debye temperature to decrease k_s. Assembling thin plates of superconducting material can also reduce k_s. A typical value of the switching ratio at 10 mK is $10^3 \sim 10^5$.

Physical properties of possible superconducting materials for the superconducting heat switch are listed in Table 2. It is also important to reduce the thermal boundary resistance at the connection between the superconducting material and the thermal link of the heat switch. All materials in Table 2 except aluminum (Al) can themselves be soldered to the thermal link made of copper or silver. Highly pure samples of lead (Pb), tin (Sn), and indium (In) are readily available. Pb has a stronger critical magnetic field, and it is thus sometimes used in environments with rather stronger fields. Since the α–β structural transformation of Sn proceeds quickly around 225 K and the structure subsequently becomes brittle, the cryostat should not be kept for a long time around this temperature. Indium has a large nuclear quadrupole interaction corresponding to an internal field of 250 mT, but the heat capacity due to this interaction is negligible in practice. The availability of high-purity In and the low melting temperature of In provide a large value of RRR over 10^4 without annealing. Zinc (Zn) and Al are popular materials for heat switches because of their lower transition temperatures and weaker critical fields. In the case of Al, both ends of the Al plates are gold plated after the oxide layer is removed, and they are mechanically connected to the thermal links.

One example of a heat switch used in our laboratory is shown in Fig. 4. We use highly pure (99.9999%) indium plates that have a residual resistivity ratio (RRR) of over 10^4 without additional annealing. Two plates with area of 5×5 mm^2 and thickness of 1 mm are soldered themselves to OFHC copper thermal links that are annealed to improve RRR to 2200. We estimate that the switching ratio k_n/k_s is $46/T^2$ and the heat leak through the heat switch in the superconducting state is about 320 pW at 10 mK. The solenoid for the superconducting heat switch is wound 2000 times around a brass bobbin with superconducting CuNi/NbTi wire of 0.121-mm diameter, resulting in a field-to-current ratio of 85 mT/A. This solenoid is anchored to the thermal link connected to the mixing chamber of the ^{3}He–^{4}He dilution refrigerator. The applied field direction is parallel to the thin plates to reduce the eddy current heating and is perpendicular to the heat flow to avoid the freezing of magnetic flux, which would lead to degradation of the switching ratio.

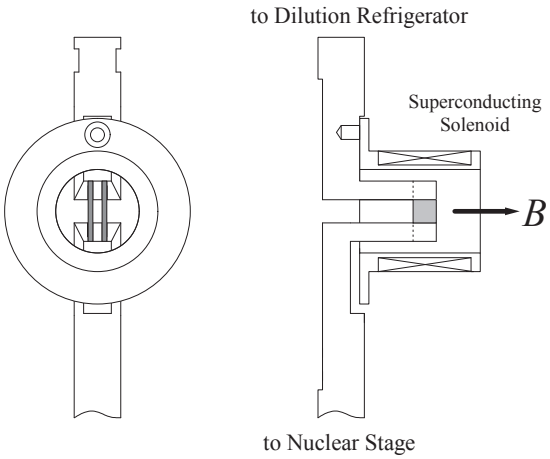

Figure 4: Schematic drawings of the superconducting heat switch and the solenoid for the application of the field in our laboratory. Two In plates with volume of $5 \times 5 \times 1$ mm^3 are soldered themselves to the copper thermal links. The superconducting solenoid applies a superconducting critical magnetic field of 29.3 mT from a current of 0.35 A for operation of the heat switch. This solenoid is anchored only to the upper side of the thermal link connecting to the precooling stage. The field direction is parallel to the thin plates of In and is perpendicular to the heat flow.

4. Thermometry

In ultra-low-temperature physics, the measurement of temperature is as important as reaching that temperature. Primary thermometers that measure low temperatures use, for example, the thermal noise of an electrical resister or the angular anisotropy of gamma rays from radioactive nuclei. However, most ultra-low-temperature laboratories make use of secondary thermometers. The resistance thermometer is most commonly used at low temperature because the sensors are readily available from manufacturers such as Lake Shore Cryotronics Inc., and the measurements are simple and easy. However, calibrated sensors are provided as low as 50 mK. It becomes difficult to get good thermal contact below this temperature, and around 10 mK, the resistance thermometer is completely unreliable. Since thermometers for measuring nuclear demagnetization temperatures are not commercially available, low-temperature laboratories make their own. Our laboratory has constructed melting curve thermometers (MCT) and platinum nuclear magnetic resonance (Pt NMR) thermometers. In this section, we describe our MCT and Pt NMR thermometers.

4.1. Melting curve thermometer

The melting pressure of ^{3}He has pronounced temperature dependence and ^{3}He can thus be used as a sensitive thermometer especially in the temperature range between 1 and 250 mK. The MCT has the significant character of several fixed points,

which are the temperatures of the minimum of the melting pressure $T_{\rm min}$, the superfluid transition $T_{\rm A}$, the A–B transition $T_{\rm AB}$ and the solid ordering transition $T_{\rm S}$ as listed in Table 3. The fixed points of Greywall are well known[24]. Fukuyama[25] and Ni[26] gave different values for the fixed-point temperatures. A "provisional low-temperature scale" from 0.9 mK to 1 K (PLTS 2000) is based on ^{3}He melting curve thermometry. The fixed points of PLTS 2000 are slightly different from those of the above researchers. The advantages of using ^{3}He are that the temperature scale is transferable between low temperature laboratories and ^{3}He is the purest substance. ^{3}He with an isotopic purity of around 10^{-5} is commercially available and ^{4}He impurities will be absorbed on the surface of the cell wall and the silver sinter heat exchanger. The drawback of the MCT is the requirement of a ^{3}He gas handling system and a fill line of ^{3}He and the large specific heat of liquid ^{3}He, although a response time of the thermometer of about 1 min can be achieved.

The melting pressure can be measured in situ using a Straty and Adams capacitive pressure gauge[27]. An automatic precision capacitance bridge can be used for measuring; however, an AC impedance bridge made of a ratio transformer and a lock-in amplifier is suitable for low-temperature measurement. To ensure small stray capacitance, we use non-microphonic coaxial cables. Two types of reference capacitors are tried. A mica capacitor is installed at 4.2 K in one cryostat. A MCT cell that has a reference capacitor was designed and constructed as shown in Fig. 5. In this setup, we can make the reference capacitor as similar to the working capacitor as possible so as to reduce temperature variation in the background signal.

Here, we describe the detail of our MCT pressure gauge. A pressure diaphragm that has a diameter of 6.5 mm and thickness of 0.3 mm is made from hardened BeCu. Movable, central and fixed capacitor plates are made from copper and have a diameter of 10 mm. The movable and fixed plates are glued to the diaphragm and guard bodies using Staycast 2850FT and cigarette paper for electrical insulation, and the central electrode is fixed at the center of the guard ring with Stycast 1266. All the surfaces of the electrodes are polished to optical flatness. The two capacitors are adjusted so as to have capacitance of about 10 pF in atmospheric conditions using a shim of about 50 μm. The capacitor plate moves more or less linearly with pressure. Sintered silver powder is used to increase the surface area and provide thermal contact between the cell body and ^{3}He through the large Kapitza resistance. Silver powder particles 70 nm in diameter were supplied by Vacuum Metallurgy Company (a branch of the ULVAC group). The powder is compressed in approximately 10 stages to ensure a homogenous silver sponge with a packing factor of one half. The cell body is made of silver or copper. In the case of the copper body, the interior of the cell body is thus plated with silver before packing the silver powder. The diaphragm and cell body are sealed with Stycast 1266.

It is necessary to calibrate the thermometer in each run because the pressure dependence of the capacitance slightly changes after warming. To reduce hysteresis, before calibration, we train the diaphragm several times at 1 K by applying pressure with a charcoal-filled cryopump, the so-called dip-

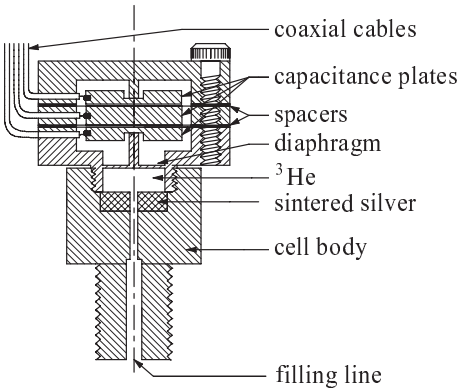

Figure 5: Schematic drawing of the ^{3}He MCT.

stick. Pressure dependence of the capacitance is calibrated at 1 K with a precise pressure gauge at room temperature. The block capillary method is used and the MCT cell is sealed with solid ^{3}He below the still of the dilution refrigerator. The pressure of the MCT cell varies with the melting curve. To prevent blocking solid ^{3}He from moving and to reduce the extra volume of ^{3}He, capillaries made from stainless steel or CuNi and having a typical outer diameter of 0.3 mm and inner diameter of 0.1 mm are used as the fill line. The sealing pressure is usually selected between 3.4 and 3.5 MPa. After the blocking of the fill line by solid ^{3}He, we apply additional pressure and seal the fill line by the valve at the top flange. Basically, the temperature is obtained from the pressure calculated using a bridge balance. We check the fixed points of the melting curve and correct the thermometer. We can obtain a ratio resolution of 10^{-8} that corresponds to a pressure resolution of $\sim$1 Pa and temperature sensitivity of $\sim 1\times10^{-3}$ around 1 mK using a driving voltage of several volts and frequency of about 1 kHz. The MCT loses the sensitivity below $T_{\rm S}$ because of the small entropy difference between solid and liquid. Although temperatures below $T_{\rm S}$ can be obtained using the temperature dependence of the melting pressure as T^4, a platinum nuclear magnetic resonance thermometer is used at lower temperatures in our laboratory.

4.2. Platinum nuclear magnetic resonance thermometer

Magnetic susceptibility of both electronic and nuclear spins has been used in thermometry because it generally follows Curie's law. Spontaneous ordering usually occurs in the millikelvin ranges for electronic spins. Thus, nuclear susceptibility is useful in the millikelvin and microkelvin regime. Platinum is the most popular material used in thermometers at such temperatures. It has one magnetic isotope, ^{195}Pt of 34% natural abundance, which has nuclear spin of one half and no quadrupole moment. The nuclear ordering temperature is believed to be less than 1 μK. As mentioned in section 2.2, the Korringa constant κ of Pt is only 29.6×10^{-3} Ks, and the nuclei and electron reach thermal equilibrium in a short time, e.g., around 30 s at $T_{\rm e}$ = 1 mK and around 1 h at $T_{\rm e}$ = 10 μK. The spin–spin relaxation time of Pt is as long as about 1 ms, and it is thus relatively easy to make NMR measurements. To measure nuclear spin

Table 3: Temperature and pressure at fixed points, and the pressure difference based on P_S on the melting curve of ^{3}He. Greywall gives the pressure difference based on P_A as 3.43380 MPa in Ref. [24]

	T_S (mK)	T_{AB} (mK)	T_A (mK)	T_{min} (mK)	P_S (MPa)	P_{AB} (kPa)	P_A (kPa)	P_{min} (kPa)	References
Greywall	0.931	1.932	2.49	-	3.439052	3.252	5.252	507.102	[24]
Fukuyama et al.	0.914	1.933	2.477	-	3.4393	3.250	5.272	–	[25]
Ni et al.	0.934	1.948	2.505	-	–	3.243	5.234	507.808	[26]
PLTS 2000	0.902	1.896	2.444	315.24	3.43934	3.32	5.27	508.21	

properties, we use the pulsed NMR technique, which is the most popular technique employed. Specifically designed electronics for the Pt NMR thermometer, PLM 4 and PLM 5 (RV Elektroniikka) are commercially available and used in many low-temperature laboratories.

The probes of the Pt NMR thermometer are generally constructed in individual laboratories. Our probes are described below. Figure 6 shows one of our NMR probes. An aligning static magnetic field of ~20 mT that is determined by the precession frequency of about 250 kHz and gyromagnetic ratio of 1.05 MHz/T is generated by a superconducting solenoid with high-magnetic-permeability metal and niobium superconducting shield. This solenoid system is thermally anchored to the mixing chamber of the ^{3}He–^{4}He dilution refrigerator. Tuning the notch coil gives field homogeneities better than 10^{-3}. The operation current is about 1 A. The Pt probe is made in the form of a brush from 3000 wires. The Pt wires with purity of 4N are commercially available. The diameter of the wire is 25 μm and is determined considering the eddy current heating and penetration of the radio-frequency field (skin depth). The Pt brush is made of annealed wires and is welded to a Pt plate. To reduce eddy current heating, it is necessary to insulate the wires. Silicone oxide is thus sputtered on the wires after welding. The Pt probe is bolted to the thermal contact post. The thermal contact post, bolts and base flange are made from silver to avoid large nuclear specific heat of Cu. These silver parts are annealed for good thermal conduction. The pulse and detection coil having inductance of about 350 μH is wound using 20-μm-diameter Cu wire and thermally anchored to the thermal contact post. This pick-up circuit is tuned to the operation frequency by the capacitor in the preamplifier. In pulsed NMR thermometry, one can measure the nuclear spin temperature from magnetization measurements using Curie's law. The electronic temperature is also determined from measurements of the spin–lattice relaxation time τ_1 and Korringa's law. However, it is noted that τ_1 is sometimes sensitive to impurities. We usually measure the magnetization using the free induction decay (FID) signal. Magnetization is calculated by integrating the FID signal in the time region that there is exponential decay due to spin–spin relaxation. The nuclear Curie law is calibrated at high temperatures with fixed points of the MCT such as T_S, T_{AB} and T_A because of uncertain factors in the magnetization measurements. Curie's law is extrapolated into the low-temperature region to measure the nuclear spin temperature.

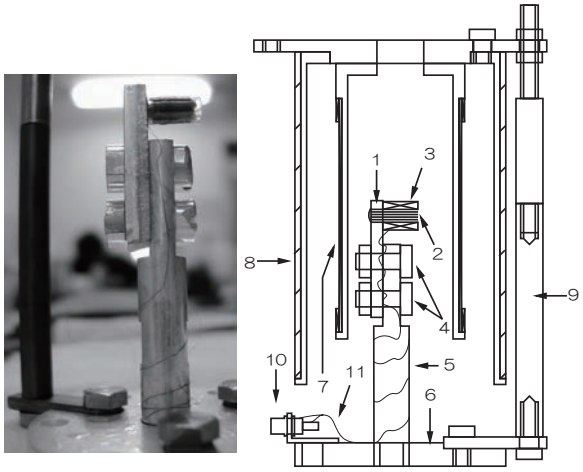

Figure 6: Schematic drawing and photograph of the platinum nuclear magnetic resonance (Pt NMR) thermometer. 1 Platinum plate. 2 Platinum brush. 3 Pulse and detection coil. 4 Silver bolts. 5 Silver thermal contact post. 6 Silver flange. 7 Superconducting solenoid with notch coils. 8 High-magnetic-permeability metal and niobium superconducting shield. 9 Vespel supports. 10 Coaxial connector. 11 Copper wires.

5. Operation of nuclear demagnetization refrigerator

In this section, we describe typical operation of our single copper nuclear demagnetization refrigerator. After precooling of the nuclear stage to 10 mK, the stage is started to demagnetize. The magnetic field is decreased exponentially with time; the procedure is divided into 8 ~ 10 steps of linear demagnetization and the rate of demagnetization is reduced in proportion to the field such as form 8 to 4 T in 8 h, then from 4 to 2 T in the same number of time, because of the lengthening the spin-lattice relaxation time. Thermalization time is necessary between steps. The fixed points of MCT are confirmed and Pt NMR thermometer is calibrated using these fixed points during demagnetization. We have to make a compromise between the lowest temperature and the large heat capacity to keep the stage for the desired length of time. The final demagnetization field and the lowest temperature, typically 10 mT and 200 μK in our refrigerator, are usually much higher than the optimal values as shown in 2.3 in order to maintain the temperature below 1 mK over one month for various measurements. We can also control the stage temperature by magnetizing and demagnetizing the magnet. The field change behaves in a nearly ideal adiabatic way, B/T is constant. Finally, the nuclear stage looses entropy

by external heat leaks, then, the heat switch is closed and precooling process would be restarted. So, the nuclear demagnetization is a 'one-shot' process different from higher temperature magnetic refrigerators. The performance in the second demagnetization is better than in the first demagnetization because the long-term-relaxation heat leak would decrease.

6. Summary

In summary, we review the basic principle, method, and requirements for the nuclear demagnetization, and present our copper nuclear demagnetization stage, indium superconducting heat switch, and thermometers used at temperatures down into submillikelvin region. The basic technique of the nuclear demagnetization has been established, however, it is necessary to construct the nuclear demagnetization system by ourselves using the suitable materials, methods, heat switches, and thermometers in accordance with measurements and temperature ranges. Thus, this technique will remain and develop in the future for cooling an appreciable amount of matter down to millikelvin or submillikelvin temperatures.

References

[1] C. J. Gorter, Physik. Z. **35**, 928 (1934).
[2] N. Kurti, F. N. H. Robinson, F. E. Simon, and D. A. Spohr, Nature **178**, 450 (1956).
[3] O. V. Lounasmaa, *Experimental Principle and Methods Below 1K* (Academic, New York, 1974).
[4] G. K. White, *Experimental Techniques in Low-Temperature Phyiscs* (Oxford University Press, London, 1959).
[5] D. S. Betts, *An Introduction to Millikelvin Technology* (Cambridge University Press, Cambridge, 1989).
[6] R. C. Richardson and E. N. Smith, *Experimental Techniques in Condensed Matter Physics at Low Temperatures* (Addison-Wesley, Redwood City, CA, 1988).
[7] F. Pobell, Physica **109 110B**, 1485 (1982).
[8] M. Schwark, F. Pobell, W. P. Halperin, Ch. Buchal, J. Hanssen, M. Kubota, and R. M. Mueller, J. Low Temp. Phys. **53**, 685 (1983).
[9] A. S. Oja, O. V. Lounasmaa, Rev. Mod. Phys. **69**, 1 (1997).
[10] M. T. Huiku, T. A. Jyrkkiö, J. M. Kyynäräinen, M. T. Loponen, O. V. Lounasmaa, and A. S. Oja, J. Low Temp. Phys. **62**, 433 (1986).
[11] P. J. Hakonen, S. Yin, and O. V. Lounasmaa, Phys. Rev. Lett. **64**, 2707 (1990).
[12] J. T. Tuoriniemi, T. A. Knuuttila, K. Lefmann, K. K. Nummila, W. Yao, and F. B. Rasmussen, Phys. Rev. Lett. **84**, 370 (2000).
[13] Y. Koike, H. Suzuki, S. Abe, Y. Karaki, M. Kubota, and H. Ishimoto, J. Low Temp. Phys. **101**, 617 (1995).
[14] J. Leib, M. Huebner, S. Götz, Th. Wagner, and G. Eska, J. Low Temp. Phys. **101**, 253 (1995).
[15] K. I. Juntunen and J. T. Tuoriniemi, Phys. Rev. Lett. **93**, 157201 (2004).
[16] T. Lang, P. L. Moyland, D. A. Sergatskov, E. D. Adams, and Y. Takano, Phys. Rev. Lett. **77**, 322 (1996).
[17] P. M. Berglund, G. J. Ehnholm, R. G. Gylling, O. V. Lounasmaa, R. P. Søvik, Cryogenics **12**, 297 (1972).
[18] R. M. Mueller, C. Buchal, H. R. Folle, M. Kubota, and F. Pobell, Cryogenics, **20**, 395 (1980).
[19] J. Xu, O. Avenel, J. S. Xia, M-F. Xu, T. Lang, P. L. Moyland, W. Ni, E. D. Adams, G. G. Ihas, M. W. Meisel, N. S. Sullivan, and Y. Takano, J. Low Temp. Phys. **89**, 719 (1992).
[20] K. Gloos, P. Smeibidl, C. Kennedy, A. Singsaas, P. Sekowski, R. M. Mueller, and F. Pobell, J. Low Temp. Phys. **73**, 101 (1988).
[21] S. A. Altshuler, JETP Lett. **3**, 112 (1966).
[22] K. Andres, and E. Bucher, Phys. Rev. Lett. **21**, 1221 (1968).
[23] H. C. Meijer, G. J. C. Bots, and H. Postma, Physica B+C **107**, 607 (1981).
[24] D. S. Greywall, Phys. Rev. **B33**, 7520 (1986), D. S. Greywall, Phys. Rev. **B31**, 2675 (1983).
[25] H. Fukuyama, H. Ishimoto, T. Tazaki, and S. Ogawa, Phys. Rev. **B36**, 8921 (1987).
[26] W. Ni, J. S. Xia, and E. D. Adams, J. Low Temp. Phys. **99**, 167 (1995).
[27] G. S. Straty and E. D. Adams, Rev. Sci. Instrum. **40**, 1393 (1969).